Mechanisms Controlling the Past, Present, and Future Trends in the South Atlantic Ocean's Heat Storage in a Set of CESM2 Large Ensemble Simulations

Maurício R. Rocha,[a] Gustavo M. Marques,[b] Frederic S. Castruccio,[b] Anna-Lena Deppenmeier,[c] Olga T. Sato,[a] and Gokhan Danabasoglu[b]

[a] *Oceanographic Institute, University of São Paulo, São Paulo, São Paulo, Brazil*
[b] *Climate and Global Dynamics Laboratory, National Science Foundation National Center for Atmospheric Research, Boulder, Colorado*
[c] *Department of Earth, Ocean and Ecological Sciences, University of Liverpool, Liverpool, United Kingdom*

(Manuscript received 11 February 2025, in final form 19 January 2026, accepted 9 February 2026)

ABSTRACT: The South Atlantic Ocean is projected to warm under the increase in greenhouse gas emissions. How much of this warming is due to the ocean or the atmosphere has been an open question. With the hypothesis that changes in the Atlantic meridional overturning circulation (AMOC) are the main mechanism explaining the South Atlantic Ocean warming, this work aims to understand the changes in the components of the heat budget in the South Atlantic Ocean (0°–34°S) during the historical and future transient periods. We examine the simulations performed as part of the Community Earth System Model (CESM), version 2, Large Ensemble project (LENS2) that follow the Coupled Model Intercomparison Project phase 6 protocols. Specifically, we analyze the heat budget between 1850 and 2100 and investigate the relationship between changes in the heat budget and changes in AMOC. Our analysis reveals that from 1850 to the 1990s, the surface heat fluxes are partially in equilibrium with the heat exchanged laterally at 34°S and the equator. Consequently, no significant trends in the heat storage rate are seen for that period. However, during the 2015–2100 future period, under the shared socioeconomic pathways 3-7.0 scenario, the heat storage rate significantly increases due to reduced northward heat transport at the equator. This reduction is attributed to the weakening of the AMOC upper cell transport. This article emphasizes the crucial role of the AMOC in regulating the heat balance in the South Atlantic and its potential to alter the basin temperature in a warming climate.

KEYWORDS: Ocean circulation; Budgets; Climate change; Climate models; Trends

1. Introduction

Strong incoming solar radiation at the equator and heat loss through outgoing radiation at the high latitudes create a radiative imbalance between these two regions (Trenberth and Solomon 1994). The meridional–vertical circulation cells in the ocean and the atmosphere reduce this thermal energy gradient (Trenberth and Caron 2001). In the ocean, this circulation pattern is known as the meridional overturning circulation (MOC), and it is obtained by integrating the ocean circulation zonally.

The overturning circulation transports physical, chemical, and biological properties between the ocean's surface and interior and among the basins, making its dynamics crucial for understanding ecosystem and climate patterns (Kuhlbrodt et al. 2007; Buckley and Marshall 2016). In the Indo-Pacific, the overturning circulations transport heat poleward in both hemispheres (Lee and Marotzke 1998; Trenberth et al. 2019; Povea-Pérez et al. 2024). However, the heat transported by the Atlantic component of the overturning circulation [Atlantic meridional overturning circulation (AMOC)] is northward across the basin, which makes AMOC a key factor for the current planetary energy balance (Marshall et al. 2014; Majumder et al. 2016; Frajka-Williams et al. 2019).

Excluding the near-surface, wind-driven circulations, AMOC comprises of two main cells: a clockwise-circulating upper cell associated with the northward transport of surface warm and saltwaters and the southward North Atlantic Deep Water (NADW) transport. The counterclockwise-circulating abyssal cell is associated with the Antarctic Bottom Water (AABW) occupying a depth range down to about 3000–4000 m. Usually, the strength of AMOC is measured by the maximum transport of the upper cell (Frajka-Williams et al. 2019). Time series of this metric is commonly used to assess changes in AMOC (Jackson et al. 2016; Danabasoglu et al. 2021; Chidichimo et al. 2023).

Since the last century, the South Atlantic Ocean has been undergoing significant ocean surface warming (Cheng et al. 2017, 2020). The increasing sea surface temperatures (SSTs) in this region are expected to be related to an AMOC weakening, which would imply a warming trend also below the surface (Barnett et al. 2005; Lee et al. 2011). As the meridional heat transport (MHT) in the basin depends on the heat transport by the AMOC upper cell (Dong et al. 2021), qualitative assumptions about changes in basin temperature and heat storage rate from different AMOC states are commonly made, taking into consideration only MHT (Sancho et al. 2015; Mecking and Drijfhout 2023). However, to close the heat budget and ensure heat conservation, one must also consider the total surface heat flux (SHF), given by the sum of the sensible (SH), latent (LH), shortwave (SW), and longwave (LW) heat fluxes. Analyzing the terms of the heat budget separately without ensuring heat

Corresponding author: Maurício R. Rocha, mauricio.rocha@alumni.usp.br

DOI: 10.1175/JCLI-D-25-0089.1

conservation can result in mixed interpretations regarding temperature changes in the basin from different climate change scenarios.

Sancho et al. (2015) analyzed MHT in some South Atlantic and Southern Ocean transects in model simulations. They concluded that in an atmosphere with high anthropogenic CO_2 concentrations, advective heat supply would decrease at 25°S due to decreased northward volume transport. However, because MHT is only one component of the heat budget, the authors could not state whether this decrease in MHT results in a decrease in heat storage north of 25°S. As the Southern Ocean is projected to warm (Cheng et al. 2022), the decrease in MHT (Sancho et al. 2015) at the southern boundary of the South Atlantic can be driven by velocity anomalies which can generate a deficit of heat entering the basin from the south (Mecking and Drijfhout 2023). Furthermore, although the Agulhas leakage is projected to increase under a warming climate (Marcello et al. 2023; Großelindemann et al. 2025), most of the heat transported by its waters is lost to the atmosphere in the South Atlantic locally (Ivanciu et al. 2021). In other words, heat transport from the south may not explain the increased heat storage rate in the basin in climate projections.

Spatial variations in SHF usually resemble SST patterns. Increased downward SHF can occur when the ocean surface warms less, as stronger ocean surface warming can release more heat into the air (Xie et al. 2010). Hu et al. (2020), using the Community Earth System Model (CESM), version 1, at nominally 1° horizontal resolution with 10 ensemble members, analyzed all heat budget components globally under greenhouse warming (freshwater perturbation and doubling CO_2 experiments). In a warmer climate, they found that in some regions of the South Atlantic, SHF anomalies coincide with negative SST anomalies. They also showed that the largest amount of excess heat due to the anthropogenic greenhouse effect will be absorbed in the Southern Ocean in a band around 55°S. Thus, the negative correlation between SST and SHF along with the decline of the AMOC highlights the need for further research to understand the future warming of the South Atlantic Ocean. Besides, their experiments used a virtual timeline to test varying CO_2 concentrations, thus making it impractical to apply these results to real-time changes, which is essentially important for decision-makers.

In water hosing experiments, where the effect of the AMOC can be isolated, the weakening of the AMOC in future climates directly impacts the position of the intertropical convergence zone through a southward shift in convection and a reorganization of the Hadley cell (Liu et al. 2020; Bellomo et al. 2023). This might occur due to a smoothing of the interhemispheric heat content gradient, as suggested by Schneider et al. (2014). Despite these studies, how much of the warming in the South Atlantic is due to the net surface heat fluxes versus the northward heat transport convergence remains largely unanswered. Here, we address this question by performing a heat budget analysis in the South Atlantic Ocean and investigate the mechanisms controlling its components for the historical period (1850–2014) and the shared socioeconomic pathways (SSPs) 3.7-0 projection (2015–2100), one of the scenarios in the Coupled Model Intercomparison Project phase 6 (CMIP6) (O'Neill et al. 2016). Our goal is to determine the causes of the recent elevated warming over the last few decades and how it will evolve until the end of this century.

This manuscript is organized as follows. Section 2 describes the datasets and the methodology used to compute the heat budget. In section 3, we present time series of the heat budget components in the South Atlantic Ocean, emphasizing the changes in the heat storage rate. We also present changes in the upper and abyssal cells of AMOC for the current and future climate, as well as the volume balance in the southern and the northern boundaries of the basin. We conclude the article with a discussion (section 4) and summary (section 5).

2. Simulations and methods

a. *Fully coupled simulations*

We use the Community Earth System Model, version 2 (Danabasoglu et al. 2020), Large Ensemble community project (LENS2) (Rodgers et al. 2021) fully coupled simulations. The large ensemble consists of many members with the same model under the same radiative forcing scenario but different initial conditions. The simulations use a nominal 1° horizontal resolution for each model component (ocean, atmosphere, sea ice, and land). LENS2 has 100 members covering the period 1850–2100. Following the protocol for the CMIP6 experiments, historical forcing is used from 1850 to 2014, followed by the SSP3-7.0 (Meinshausen et al. 2020) forcing from 2015 to 2100.

SSP3-7.0 is one of the five high-priority scenarios for the Sixth Assessment Report of the Intergovernmental Panel on Climate Change (IPCC). It is a medium–high reference scenario with one of the highest methane and air pollution precursor emissions (Meinshausen et al. 2020), high aerosol emissions, and land-use change (O'Neill et al. 2016). Under this scenario, the CO_2 emissions double by 2100, and CO_2 concentrations are projected to reach approximately 867 ppm, resulting in an average global radiative forcing increase of 7.0 W m^{-2}. We defined the periods 1990–2020 and 2070–2100 to represent the average state of the present and future climate, respectively.

The LENS2 spread is generated by a combination of micro and macro initialization approaches that also sample different AMOC phases (Rodgers et al. 2021). Each simulation has its own random sequence of internal variability, superimposed upon a common forced response (estimated by the ensemble mean). One of the advantages of such large ensemble products is that internal variability can be isolated from the external forcing (forced variability) by averaging over all the members (Deser et al. 2012, 2020; Murphy et al. 2021). The results in this study refer to the ensemble mean over all 100 LENS2 members, representing the forced response. For reference on internal variability, we compute the ensemble spread, which means the interval between the maximum and minimum values of the members, and select randomly only one member for comparisons. Our analysis is based on monthly mean output.

To assess the statistical significance of linear trends in the time series, we apply a nonparametric Monte Carlo approach. For each original time series, we compute the linear trend using

ordinary least squares regression. To construct the null distribution, we generate 10 000 surrogate time series by randomly shuffling the original series, thereby preserving its mean and standard deviation while removing temporal autocorrelation. An empirical two-tailed p value is estimated as the fraction of surrogate slopes whose absolute values were greater than or equal to the absolute value of the "truth" time series. A trend is statistically significant at the 95% confidence level if the empirical p value is less than 0.05. Additionally, we calculate the 95% confidence interval of the surrogate slope distribution (2.5th and 97.5th percentiles) to verify whether the observed trend lies outside this interval, providing a complementary measure of statistical significance.

b. Methods

The ocean heat budget is computed using the three-dimensional heat conservation equation; that is, fluxes through all boundaries are balanced by heat content changes in our domain. The total heat budget in a volume (mass)-conserving ocean is defined as

$$\mathrm{SHF} - \mathrm{MHTD} = \mathrm{HSR}, \tag{1}$$

where SHF is the net heat flux over the surface due to exchanges through the air–sea interface (with a positive sign directed toward the ocean). MHTD is the MHT difference between two parallel zonal sections (a proxy for the divergence), and HSR is the heat storage rate in the ocean's interior, i.e., the time derivative of ocean heat content, all in watts (W). The heat exchanged at the ocean floor is considered to be negligible. The sum of the three terms—MHTD, SHF, and HSR—equals zero following Eq. (1). To verify the correctness of our residual-based approach, we had also computed HSR independently based on instantaneous temperature fields from model simulations, essentially producing the same HSR values.

SHF is calculated by integrating the contributions of the surface heat flux components over the surface area as follows:

$$\mathrm{SHF} = \int_{y_2}^{y_1}\int_{x_2}^{x_1}(\mathrm{SW} + \mathrm{LW} + \mathrm{LH} + \mathrm{SH})dxdy, \tag{2}$$

where x is the zonal direction, with x_1 and x_2 representing the eastern and western limits of the basin, respectively. The y is the meridional direction, with y_1 and y_2 representing the northern and southern limits, respectively.

The heat flux across an oceanic zonal section is the MHT, calculated as

$$\mathrm{MHT}(y) = \rho_0 C_p \int_{x_2}^{x_1}\int_{z_2}^{z_1} v\theta dz dx, \tag{3}$$

where z is the vertical direction, positive upward, with z_1 and z_2 representing the surface and bottom, respectively. The $\rho_0 = 1026$ kg m^{-3} is the reference density, and $C_p = 3996$ J (kg °C)$^{-1}$ is the specific heat of seawater at constant pressure. The $v(x, y, z)$ is the meridional velocity component, and $\theta(x, y, z)$ is the potential temperature (°C) or simply temperature henceforward.

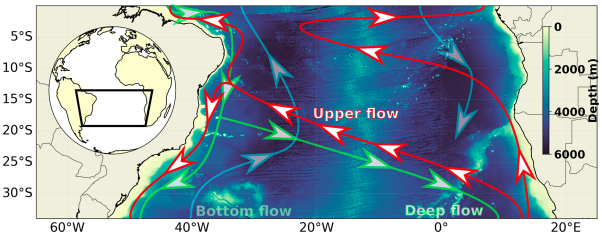

FIG. 1. Regional map of the South Atlantic Ocean. The region of study is defined as the area between 0° and 34°S (black box in the inset). The arrows represent the main water flow routes in the basin for the upper ocean (red; 0–1000-m depth), deep ocean (green; 1000–4000-m depth), and abyssal/bottom ocean (blue; 4000–bottom).

The South Atlantic Ocean is a closed basin in the zonal direction. We choose the equator and 34°S as the limits of our study area for the heat flux calculations with the assumption that volume is conserved in this domain. Equation (1) is applied in the area highlighted in Fig. 1 where its components are limited zonally by the South American and African continents, meridionally by the equator and the latitude of 34°S, and vertically from the surface to the bottom of the ocean. The difference in MHT between the two meridional limits of the study domain (equator minus 34°S) is MHTD in Eq. (1). We decompose MHT into contributions from the time mean ($\overline{\mathrm{MHT}}$) and fluctuations from that mean (MHT′) for the period between 1850 and 2014 (historical) and between 2015 and 2100 (SSP3.7-0). Thus, the temperature and the meridional velocity can be rewritten as $\theta = \overline{\theta} + \theta'$ (°C) and $v = \overline{v} + v'$ (m s^{-1}), respectively. Because ρ_0 and C_p are constants, MHT can be decomposed as

$$\mathrm{MHT} = \rho_0 C_p \int_{x_2}^{x_1}\int_{z_2}^{z_1}(\overline{v}\,\overline{\theta} + \overline{v}\theta' + \overline{\theta}v' + v'\theta')dzdx, \tag{4}$$

where $\overline{v}\,\overline{\theta}$ is constant in time per period (1850–2014 and 2015–2100), $\overline{v}\theta'$ represents MHT that arises from temperature anomalies advected by the mean flow, $\overline{\theta}v'$ is the contributions from advection of the mean temperature by velocity fluctuations, and $v'\theta'$ are the MHT anomalies caused by meridional velocity and temperature fluctuations interacting with each other. Equation (4) quantifies the importance of temperature versus meridional velocity for the variability and trends of MHT.

To understand how the different parts of the circulation contribute to changes in the AMOC, we decompose the circulation's volume transport into the upper, deep, and bottom layers (Fig. 1) and into two distinct areas: the southward or northward flow along the western boundary and the central and eastern sides of the basin across 34°S and at the equator. The meridional boundary is set to dynamically differentiate the integrated transports in the western boundary current–related part from the rest of the basin. This boundary marks the longitude at which the southward (northward) transport reverses from negative (positive) to positive (negative) values. This approach is applied to each vertical layer, meaning that the boundaries

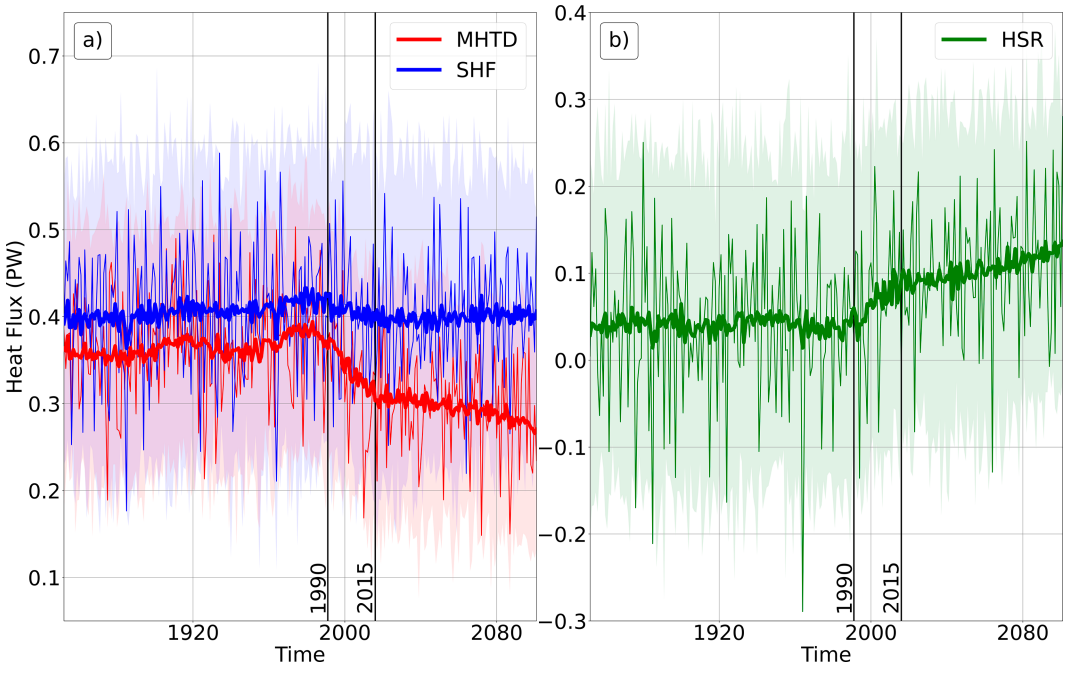

FIG. 2. Time series of annual-mean and ensemble-average (a) total SHF and MHTD between the northern (0°) and southern (34°S) boundaries of the South Atlantic Ocean (see Fig. 1). (b) HSR is computed via Eq. (1). Positive SHF indicates flux from the atmosphere to the ocean. The thin lines represent the annual mean for a random member. The vertical solid black lines mark the years 1990 and 2015. The shadings represent the respective ensemble spreads.

may not align between different layers because the boundary depends on the sign reversal of the transports. The vertical layers are roughly defined to separate the surface circulation, which includes the Brazil Current and the North Brazil Current, from the deep circulation, which includes the transport of NADW by the deep western boundary current (DWBC), and from the bottom circulation, which includes the northward transport of AABW. We conducted sensitivity tests by adjusting the boundaries of these vertical layers, and the interpretation of the results remained consistent. We perform this analysis for the present (1990–2020) and future (2070–2100) climates and subtract the present climate from the future climate to highlight future changes in the volume transport at those latitudes.

3. Results

a. *Heat budget in the South Atlantic Ocean*

In this section, we analyze the changes in each component of the heat budget in the South Atlantic Ocean. Figure 2 shows the time series of the total SHF [Eq. (2)], the MHTD between the equator and 34°S, and the HSR [Eq. (1)]. From 1850 until approximately 1990, the heat entering the basin from the surface (SHF $>$ 0) is partially balanced by the heat exported to the North Atlantic Ocean at the equator (MHTD $>$ 0) (Fig. 2a). The linear trend of MHTD and SHF is 1.63 $\pm$ 0.19 TW decade^{-1} (p = 0.0001) and 1.67 $\pm$ 0.57 TW decade^{-1} (p = 0.0001), respectively. The HSR in the basin does not show a significant linear trend (0.05 $\pm$ 0.21 TW decade^{-1}, p = 0.8148) and oscillates around 0.04 PW (Fig. 2b). In contrast to the earlier period, the period between 1990 and 2015 displays the strongest trends over the entire period analyzed: -25.37 ± 2.15 TW decade^{-1} (p = 0.0001), -6.34 ± 2.22 TW decade^{-1} (p = 0.0089), and 19.02 $\pm$ 3.25 TW decade^{-1} (p = 0.0001), respectively, for MHTD, SHF, and HSR, all significant at the 95% level. Therefore, from around the 1990s, the South Atlantic Ocean began to increase its heat content at a rate much higher than the estimates between 1850 and 1990.

In the SSP3-7.0 scenario (starting in 2015), the balance between MHTD and SHF changes again: SHF increases (0.85 $\pm$ 0.35 TW decade^{-1}, p = 0.0166), mainly due to increased solar radiation reaching the surface, which results from a decrease in cloud cover and thickness (Figs. A1 and A2 in the appendix). The MHTD decreases, but at a greater rate (-3.86 ± 0.30 TW decade^{-1}, p = 0.0001) compared to SHF. Consequently, HSR continues to increase albeit at a lower rate (4.71 $\pm$ 0.37 TW decade^{-1}, p = 0.0001) mainly because of the reduction in the MHTD. Therefore, the relative contributions of the MHTD and SHF trends to the HSR trend in the SSP3-7.0 projection are 82% and 18%, respectively. The accumulation of heat in the South Atlantic Ocean continues until the end of the twenty-first century. We can attribute these trends to forcings in the model, as the preindustrial runs do not show significant trends (not shown). For the period between 1990 and 2015, 100% of the trend in HSR is explained by MHTD. These trends are significant at the 95% confidence level.

b. *Meridional heat transport*

We have shown that MHTD is the primary mechanism explaining the trend in HSR between 1990 and 2015, as well as

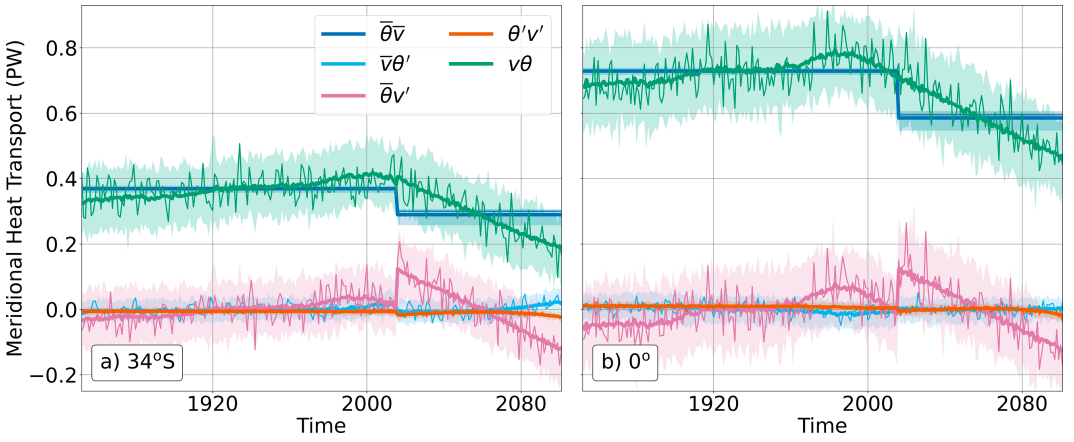

FIG. 3. Time series of annual means and ensemble averages of the MHT components from Eq. (4) between the years 1850–2100. The terms are integrated vertically and zonally at (a) 34°S and (b) 0°. The thin lines represent the annual mean for a random member. The shadings represent the respective ensemble spreads.

in the SSP3-7.0 scenario. In this section, we decompose MHT into its components ($\overline{v}\overline{\theta}$,$\overline{v}\theta'$,$\overline{\theta}v'$,$\theta'v'$) from 1850 to 2100. This allows us to determine whether changes in the temperature or velocity structure drive the trends in MHTD during both the historical and future projection periods.

Figures 3a and 3b show the time series of the terms in the MHT decomposition [Eq. (4)] at 34°S and 0°, respectively. At both latitudes and in the SSP3.7-0 scenario, while the MHT magnitudes are dictated by the advection of the mean temperature by the mean velocity ($\overline{\theta}\overline{v}$), the trends in MHT are determined by the advection of the mean temperature by the velocity anomalies ($\overline{\theta}v'$). The contributions of the other two terms ($\overline{v}\theta'$ and $\theta'v'$) at both latitudes are negligible, with no discernible trends. Thus, the difference in MHT between the northern and southern boundaries of the South Atlantic Ocean, controlled by $\overline{\theta}v'$, explains the increase in HSR. During the historical period, the trend in $\overline{\theta}v'$ also closely matches that of the full $v\theta$ term.

The total MHT at the equator (Fig. 3b) is larger than at 34°S (Fig. 3a), and at both latitudes, the trend in MHT is negative between 2015 and 2100. For the MHTD trend to be negative, the decrease in MHT at the equator and 34°S must occur at different rates. To confirm that this is indeed the case, we now investigate MHT for both latitudes (Fig. 4). The reduction in the MHT magnitude trend is larger at 0° (-29.62 ± 0.29 TW decade^{-1}, $p = 0.0001$) than at 34°S (-25.76 ± 0.17 TW decade^{-1}, $p = 0.0001$); in other words, the MHT at the equator decreases faster than at 34°S, which means less heat is being exported northward across the equator. The difference in the MHT trend for the two latitudes explains the trend seen in MHTD (Fig. 4); that is, according to the LENS2 projection, the South Atlantic Ocean gains heat at the rate of 3.86 ± 0.30 TW decade^{-1} ($p = 0.0001$) because, primarily, of a reduction in the MHT at the equator. Furthermore, the maximum value of MHT occurs first at the equator (1982) and 20 years later (2002) at 34°S. This suggests that the weakening signal of this transport moves from north to south.

c. *Changes in AMOC*

So far, we have shown that the meridional volume transport anomaly controls the MHT trends in the LENS2 SSP3-7.0 ensemble mean. In addition, the increase in HSR in the LENS2 SSP3.7-0 simulations is because the South Atlantic Ocean exports less heat to the North Atlantic. In this section, we investigate whether and if so, how the volume transport changes are associated with AMOC.

To investigate whether the most significant changes in AMOC occur at the equator, we analyze the difference in AMOC transports at 0° and 34°S for the 1990–2020 and 2070–2100 periods (Fig. 5). The AMOC transport in the upper cell declines more strongly at the equator than at 34°S. Figure 5 also shows that while the magnitude of the AMOC transport

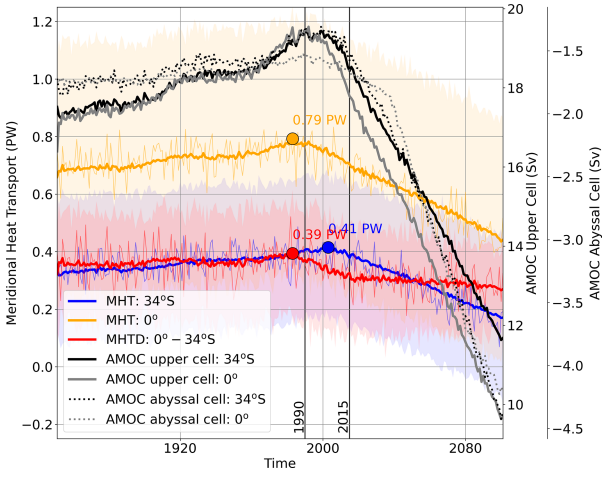

FIG. 4. Time series of annual-mean and ensemble-average MHT (thick solid lines) at 0° and 34°S, along with the corresponding MHTD between these latitudes. The year of maximum MHT between 1850 and 2100 is shown. The thin yellow, blue, and red lines represent the annual-mean MHT for a random member. The vertical solid black lines mark the years 1990 and 2015. The shadings represent the respective ensemble spreads. Additionally, the time series of annual- and ensemble-mean AMOC strength for the upper (solid lines) and abyssal (dotted lines) cells at 0° and 34°S are shown in black and gray, respectively.

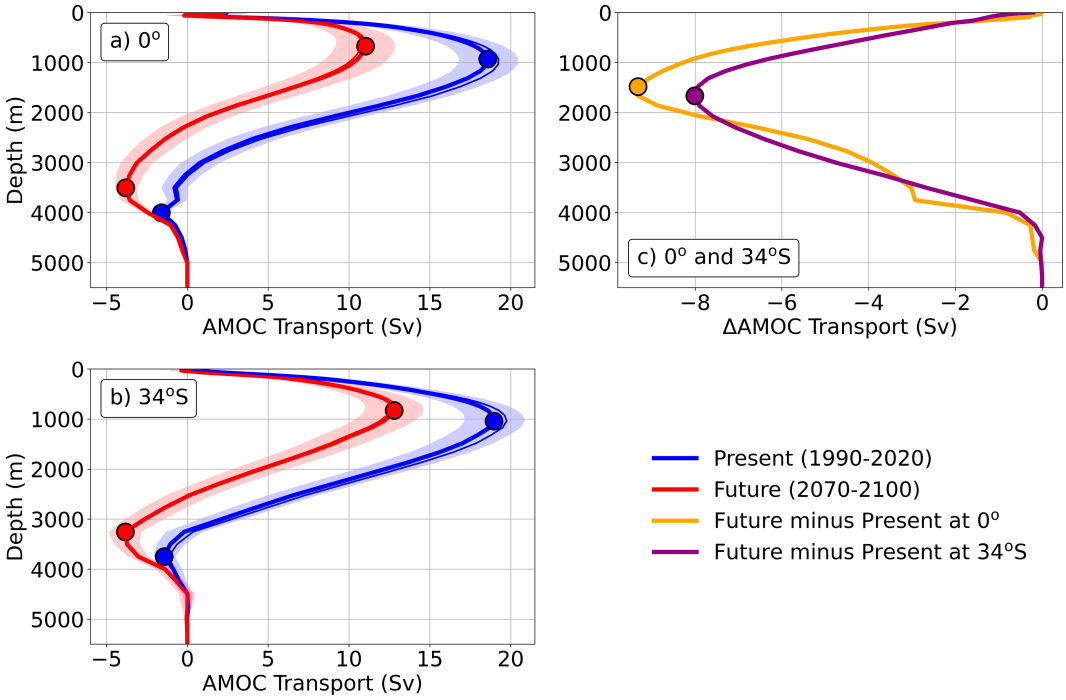

FIG. 5. Time-mean and ensemble-average AMOC transport profiles for the 1990–2020 (blue) and 2070–2100 (red) periods at (a) 0° and (b) 34°S. The maximum and minimum values are highlighted on each profile with a dot. These values mark the strength of the upper and abyssal cells of the AMOC, respectively. The thin lines represent the annual-mean AMOC transport for a random member. The shadings represent the respective ensemble spreads. (c) The difference (Δ AMOC transport) between the future and present climate for the ensemble mean at the equator and at 34°S.

in the upper cell decreases, the magnitude of the abyssal cell increases at both latitudes in the future period. Moreover, both the upper and abyssal cell maximum transports shift to shallower depths, accompanied by a contraction and expansion of the upper and abyssal cells, respectively. Over time, it is also possible to verify these changes in the strength of the AMOC cells (Fig. 4). As shown in the previous sections, these changes lead to corresponding changes in the heat budget and transports. Because the volume transport anomalies play a crucial role in controlling the changes in MHT, we argue that the AMOC is the primary mechanism driving the HSR changes in the South Atlantic Ocean.

We now investigate the decomposition of the circulation into the upper, deep, and abyssal waters to demonstrate the importance of the near-surface currents in driving ocean heat transport (Figs. 6 and 7). For the present climate, the integrated volume transports between the surface and 1000 m, between 1000 and 4000 m, and between 4000 m and the bottom of the ocean are 17.4 Sv (1 Sv $\equiv 10^6$ m^3 s^{-1}) (17.4 Sv), −19.5 Sv (−20.08 Sv), and 1.1 Sv (1.65 Sv), respectively, at 34°S (equator). For the future climate, the values are 10.8 Sv (9.3 Sv), −13.6 Sv (−12.54 Sv), and 1.9 Sv (2.48 Sv) for the upper, deeper, and abyssal ocean, respectively, at 34°S (equator). The differences between the two periods analyzed at both latitudes (Fig. 6b and Fig. 7b) indicate that in the upper ocean, the western side represents the most significant weakening of the AMOC as it has a southward volume transport anomaly of −3.8 and −9.9 Sv at 34°S and the equator, respectively. The central and eastern sides of the basin together generate a transport anomaly of −2.8 Sv at 34°S (1.8 Sv at the equator). In the deeper and abyssal oceans, the central and east sides of the basin represent the most important changes in the AMOC transport at 34°S, as they show volume transport anomalies of 3.4 and 0.7 Sv, against 2.5 and 0.1 Sv on the western side, respectively (Figs. 6d,f). Thus, AMOC changes in the upper ocean at 34°S are most prominent on the west side (58% of the changes), while for the deeper and abyssal oceans, the central and eastern sides of the basin are the most prominent regions (58% and 88% of the changes, respectively, for the deeper and abyssal oceans). At the equator, the most prominent changes continue on the western side of the basin for the deeper layer (7.3 Sv against 0.24 Sv) and at the bottom (0.7 Sv against 0.13 Sv).

Last, we compute the mixed layer depth (MLD; defined using a 0.03 kg m^{-3} density criteria) anomaly (ΔMLD) between the future (2070–2100) and present (1990–2020) climates (Fig. 8). The most significant changes in MLD occur in the North Atlantic (a shoaling of ∼−400 m) compared to the Southern Ocean (a shoaling of ∼−70 m). In some areas of the Southern Ocean, MLD is projected to deepen by about 20 m. The shoaling of the MLD in the North Atlantic is consistent with the weakening of transport in the upper cell of the AMOC.

4. Discussion

Most of the excess heat from the anthropocentric greenhouse effect will be absorbed through the surface in the

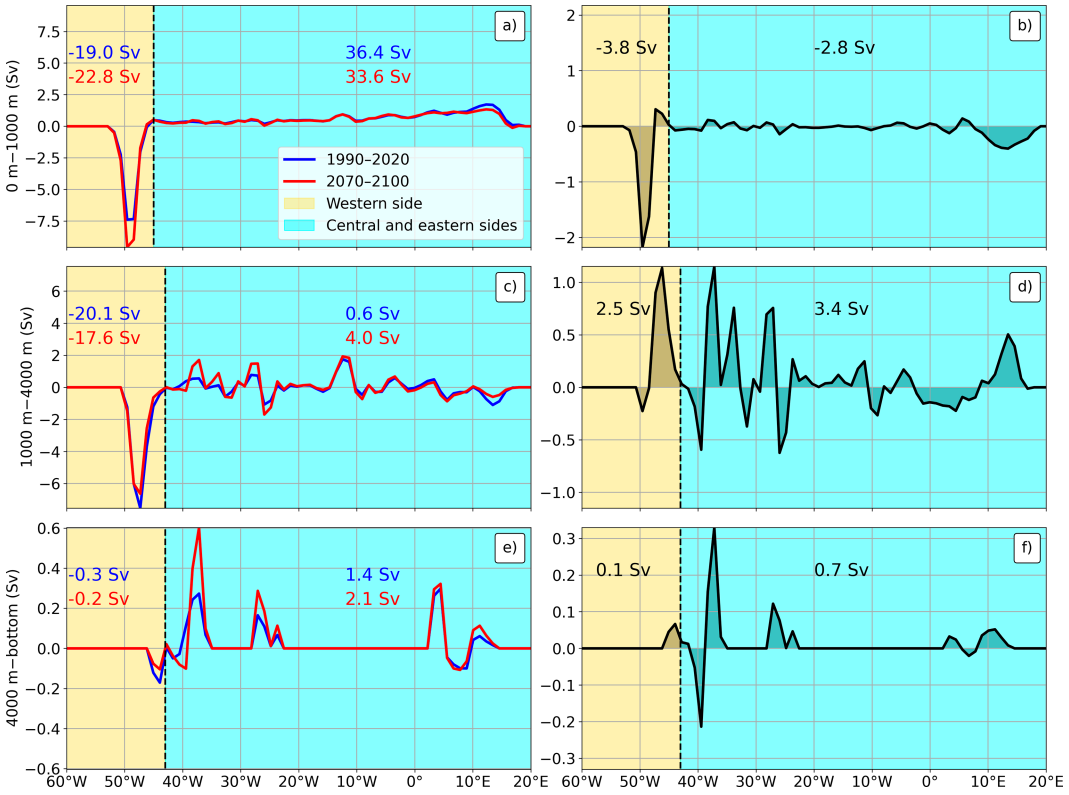

FIG. 6. (left) Time-mean and ensemble-average meridional volume transport (Sv) during the present (1990–2020) (blue line) and the future (2070–2100) climates (red line), integrated between the indicated layers at 34°S. (right) The respective meridional volume transport differences for 2070–2100 minus 1990–2020 for each layer. The numbers given in the panels indicate the total aggregated transports.

Southern Ocean, around 55°S, and transported and stored in the tropics (Hu et al. 2020). This highlights the potential influence that ocean currents have on the increase in HSR in the South Atlantic Ocean. In this basin, the meridional overturning circulation is responsible for transporting heat toward the equator in the past, the present, and the future climate. The question of whether the increase in HSR is due to the changes in surface fluxes or South Atlantic basin receiving more heat from the south or losing less heat to the north or a combination of these is addressed in this article.

Our analysis indicates that the increase in HSR in the South Atlantic Ocean is primarily due to the basin exporting less heat from south to north at the equator. The net surface heat flux increases downward due to a downward increase in shortwave heat fluxes, which result from a decrease in cloud cover and thickness, but the changes in surface heat fluxes are much smaller than the changes in meridional heat transports. Finally, we have shown that in the future climate (2070–2100), the transports in the upper and abyssal cells of the AMOC shift to shallower depths accompanied by a contraction and expansion of the upper and abyssal cells, respectively, in agreement with studies about the AMOC under different CO_2 forcings (e.g., Ma et al. 2021). This could indicate heating in the upper layer and cooling in the lower layer.

The regions of maximum NADW formation coincide with the areas of deeper MLD in the Nordic seas and Labrador Sea (Danabasoglu et al. 2014). Thus, changes in MLD in these regions are proxies for the weakening or strengthening of the transport of the AMOC upper cell. Indeed, MLDs become significantly shallower in the future climate (Fig. 8a) which implies less NADW formation and a weaker AMOC. This indicates that, within the time frame analyzed in this study, the changes in the AMOC in the South Atlantic Ocean likely originate in the northern regions. Therefore, AMOC changes are connected with the MLD changes in the northern North Atlantic.

A likely driver of shallow MLDs and subsequent AMOC weakening in the North Atlantic is the change in surface buoyancy fluxes around the North Atlantic subpolar gyre. In a warming climate with elevated CO_2 levels, disruptions in the surface heat balance are expected (Gregory et al. 2005). However, in the subpolar gyre, density is more sensitive to salinity variations than to those of potential temperature. A reduction in surface density enhances stratification, inhibiting deep convection and reinforcing a feedback loop that further weakens AMOC transport.

Freshening in the subarctic has been reported as an important mechanism of AMOC weakening (Bamber et al. 2018; Pontes and Menviel 2024). An increase in freshwater input may be due to the melting of sea ice and continental ice in high latitudes (Sévellec et al. 2017; Bamber et al. 2018; Larocca et al. 2023; Millan et al. 2023). In multicentennial AMOC variability, the

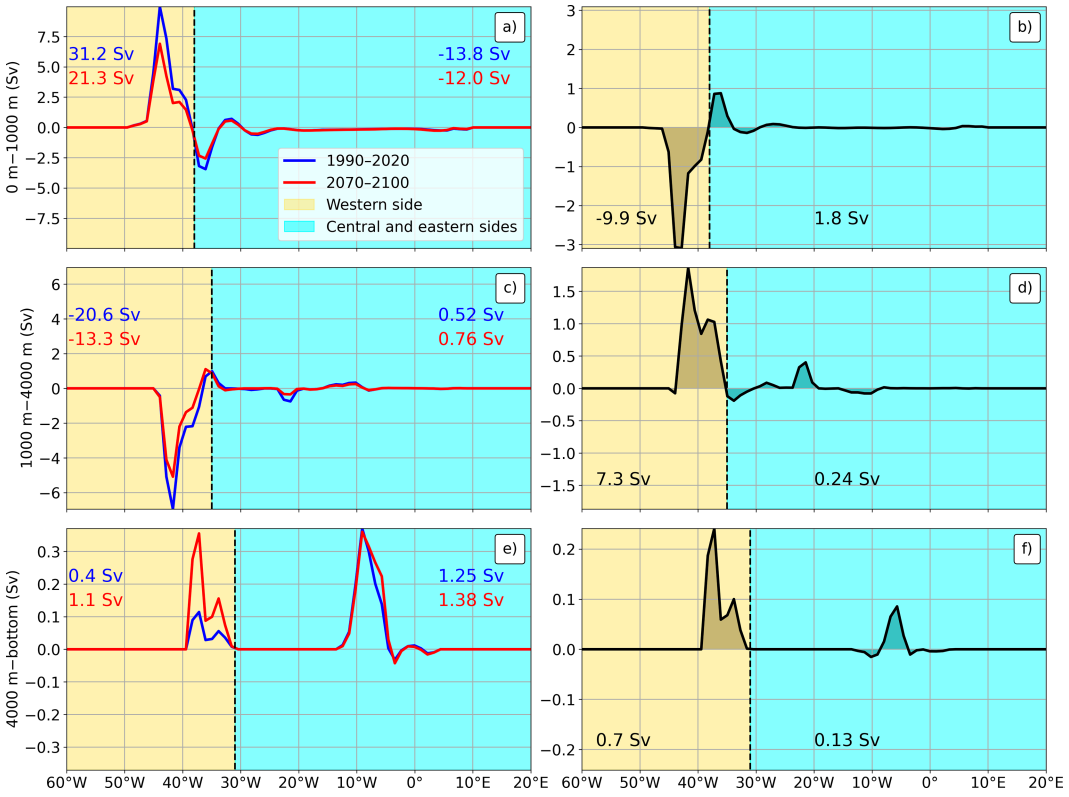

FIG. 7. As in Fig. 6, but at the equator.

freshening of the ocean due to high-latitude precipitation can also play an important role (Mehling et al. 2023). The southern limit of the Atlantic Ocean is thought to be a critical latitude for freshwater transport divergence throughout the whole basin impacting AMOC states and their stability (Van Westen et al. 2024).

The AMOC abyssal cell includes the transport of AABW, suggesting that its strengthening may be directly influenced by processes in the Southern Ocean. In the South Atlantic Ocean, we found that the strengthening of the AMOC abyssal cell is driven primarily by the intensification of northward bottom water transport. Notably, this increase in abyssal cell transport results from enhanced northward volume transport of deep waters in response to a warming climate. This process may be linked to increased deep-water formation or a compensatory response to the weakening of the AMOC upper cell due to volume conservation. However, the underlying mechanisms driving these changes require further investigation—especially in light of recent evidence of a weakening in AABW transport (Li et al. 2023; Biló et al. 2024) and the fact that in CMIP5 models, an overly weak NADW transport is associated with enhanced AABW formation (Wang et al. 2014).

We identified positive anomalies in northward volume transport within the abyssal layer (Fig. 6f), indicating a possible enhanced transport of AABW. This aligns with the findings of Wang et al. (2014), which indicate that a weaker NADW transport is linked to increased AABW formation. However, Li et al. (2023), based on high-resolution simulations of the Southern Ocean, suggest a future weakening of AABW formation. Interestingly, this weakening coincides with abyssal warming in the Southern Ocean, yet cooling in the South Atlantic and North Atlantic bottom layers. Our results also indicate a decline in abyssal temperatures in the South Atlantic Ocean (not shown), accompanied by an increase in the northward transport of cool waters along the ocean bottom. Yet, this abyssal cooling only partially mitigates the overall warming of the basin, as the dominant signal in the HSR positive trends is the weakening and contraction of the AMOC upper cell.

5. Summary and conclusions

In this article, we compute the South Atlantic Ocean heat budget for the historical period (1850–2014) and for the SSP3-7.0 projection (2015–2100) in the 100-member CESM LENS2 simulations to determine which term (total surface heat flux and meridional heat transport difference) is responsible for the increase in the heat storage rate in the basin. We analyze the forced signal of the simulations by calculating the ensemble mean and decomposing heat transport into averages and anomalies of velocity and temperature. We also decompose the volume transport in different sectors of the basin to better understand the anomalies in AMOC transport, which, by our hypothesis, would be responsible for the changes in the heat budget.

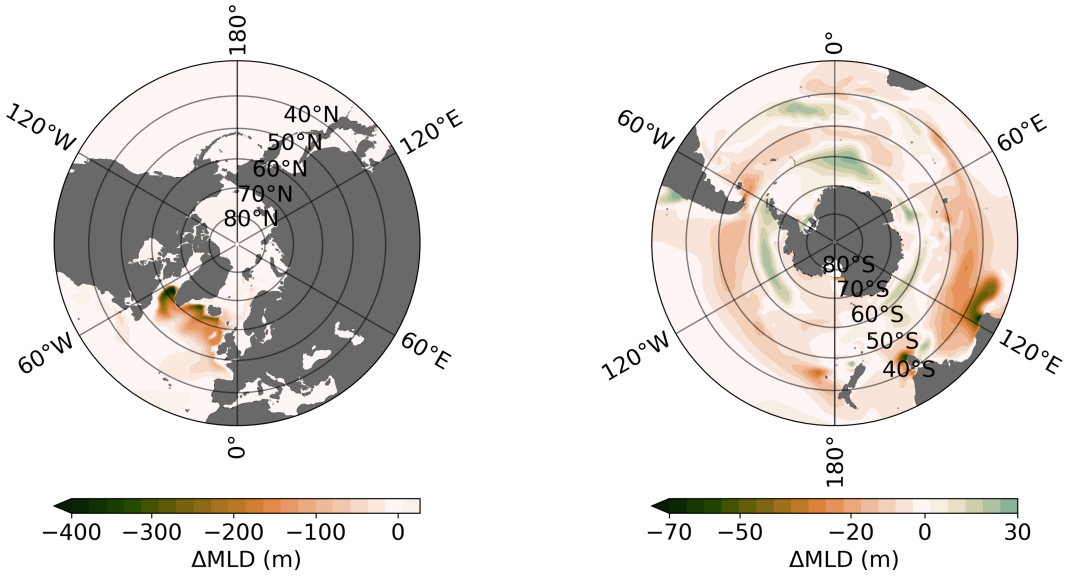

FIG. 8. Difference in the MLD, defined using a 0.03 kg m^{-3} density criterion, between the future (2070–2100) and present (1990–2020) climates (Δ MLD).

We show that up to the 1990s, the heat flux entering the South Atlantic Ocean (0°–34°S) from the surface and the southern boundary is balanced by heat export across the equator. After the 1990s, there has been a significant reduction in heat export across the equator. This is the primary reason for the increase in HSR in the SSP3-7.0 scenario simulations. The reduction in MHT is not associated with a decrease in temperature, in agreement with Mecking and Drijfhout (2023), but, instead, with a reduction in northward volume transport, i.e., a weakening of the AMOC upper cell's transport. The weakening of this transport explains the convergence anomalies in MHT.

Throughout the twenty-first century, the AMOC upper cell has been weakening and contracting, and the abyssal cell has been strengthening and expanding in the South Atlantic Ocean. The weakening of the upper branch is consistent with the shoaling of MLD, a proxy for convection in the NADW formation region. The result is a weakening of the DWBC. The strengthening of the AMOC abyssal cell, i.e., the AABW cell, in the South Atlantic Ocean is primarily driven by the northward transport of deep water. This finding highlights the need for further investigation into the role of the Southern Ocean in modulating future changes in the AMOC abyssal cell, particularly in response to shifts in bottom water formation, buoyancy fluxes, and climate-driven circulation changes.

Acknowledgments. This study was funded in part by Fulbright Brazil, the Fulbright Scholarship Board, and the Bureau of the Educational and Cultural Affairs of the United States (U.S.) Department of State for the scholarship granted to MRR as part of the Doctoral Dissertation Research Award program. This study was also funded by the Coordenação de Aperfeiçoamento de Pessoal de Nível Superior—Brasil (CAPES)—Finance Code 001. Finally, this study is under the scope of Project SAMBAR/SAMOC, funded by the Fundação de Amparo à Pesquisa do Estado de São Paulo (Ref. 2017/09659-6), as well as Projects Abyssal-AI (Ref. 444319/2024-7) and SPARC (Ref. 403892/2024-4), funded by the Conselho Nacional de Desenvolvimento Científico e Tecnológico. We acknowledge the CESM2 Large Ensemble Community Project and supercomputing resources provided by the IBS Center for Climate Physics in South Korea. We appreciate the resources and facilities provided by the University of São Paulo, Brazil, and the U.S. National Science Foundation (NSF) National Center for Atmospheric Research (NCAR), United States. We thank Drs. Frank Bryan, Michael Levy, Shenfu Dong, Cecile Hannay, and Keith Lindsay for their technical support, discussions, and data sharing. This material is also based upon work supported by NSF NCAR, which is a major facility sponsored by the NSF under Cooperative Agreement 1852977. Computing and data storage resources, including the Cheyenne supercomputer (https://doi.org/10.5065/D6RX99HX), were provided by the Computational and Information Systems Laboratory of the U.S. NSF NCAR. The authors declare no conflict of interest.

Data availability statement. The CESM LENS2 datasets are available at https://www.earthsystemgrid.org/dataset/ucar.cgd.cesm2le.output.html.

APPENDIX

Cloud and Surface Heat Flux Analysis

In this appendix, we provide additional context for the analysis of cloud properties and surface heat fluxes over the South Atlantic region, as shown in Figs. A1 and A2.

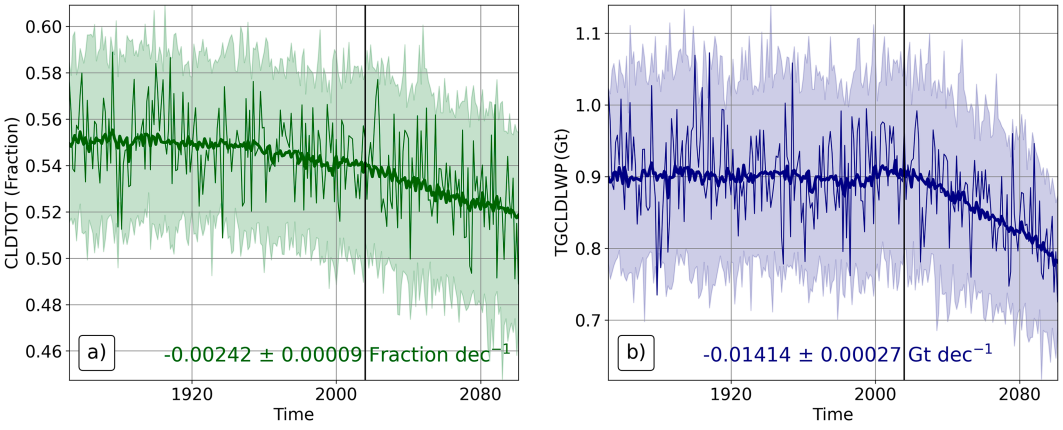

FIG. A1. Time series of annual means and ensemble averages of the (a) vertically integrated total cloud (CLDTOT) and (b) total gridbox cloud water path (liquid and ice) (TGCLDLWP) in the South Atlantic area (see Fig. 1). The thin lines represent the annual mean for a random member. The shadings represent the respective ensemble spreads.

We used two variables from the atmospheric component of the model: the vertically integrated total cloud (CLDTOT) and the total gridbox cloud water path (liquid and ice) (TGCLDLWP). The first variable, CLDTOT, represents the fractional cloud cover within the study area, providing an estimate of the average cloudiness. The second variable, TGCLDLWP, serves as a proxy for cloud thickness, as it represents the total amount of liquid and ice water integrated vertically and horizontally over the area.

Both CLDTOT and TGCLDLWP exhibit a negative linear trend toward the end of the twenty-first century (see Fig. A1), suggesting a decrease in total cloud coverage and cloud water content in the future climate. This decline is very likely to contribute to the increasing trend in incident shortwave (SW) (solar) radiation, and consequently, to the rise in total surface heat flux (SHF). This interpretation assumes that variations in solar output due to orbital changes or solar flares are negligible over the considered time scale.

Figure A2 presents the sum of surface heat flux components over the South Atlantic from 1850 to 2100 under the SSP3-7.0 scenario. The total SHF shows an increasing trend of 0.85 ± 0.35 TW decade^{-1}, indicating enhanced oceanic heat uptake in the future. Conversely, the sum of outgoing radiation components—comprising downward longwave (LWDW) radiation, upward longwave (LWUP) radiation, sensible heat flux (SH), and latent heat flux (LH)—shows a decreasing trend of 0.25 ± 0.32 TW decade^{-1}. Meanwhile, the incoming SW radiation increases at a rate of 0.61 ± 0.23 TW decade^{-1}.

Both the increase in SW and the decrease in outgoing fluxes contribute to the overall SHF increase, but the SW component plays a more dominant role. Moreover, the SW trend exhibits a smaller associated uncertainty, whereas the trend in outgoing radiation is not statistically significant. These findings further support the hypothesis that reduced cloudiness drives enhanced solar radiation and surface heat flux in the South Atlantic Ocean.

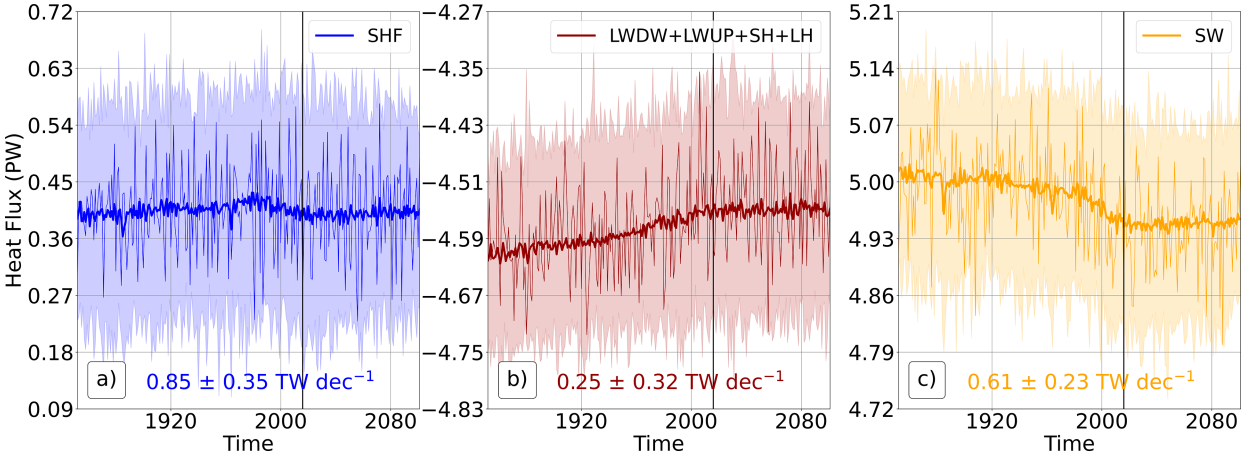

FIG. A2. Time series of annual means and ensemble averages of the (a) total SHF and (b) the sum of LWDW radiation, LWUP radiation, SH flux, and LH flux. (c) The SW radiation. The thin lines represent the annual mean for a random member. The shadings represent the respective ensemble spreads. Positive values indicate flux directed toward the ocean.

REFERENCES

Bamber, J. L., A. J. Tedstone, M. D. King, I. M. Howat, E. M. Enderlin, M. R. van den Broeke, and B. Noel, 2018: Land ice freshwater budget of the Arctic and North Atlantic Oceans: 1. Data, methods, and results. *J. Geophys. Res. Oceans*, **123**, 1827–1837, https://doi.org/10.1002/2017JC013605.

Barnett, T. P., D. W. Pierce, K. M. AchutaRao, P. J. Gleckler, B. D. Santer, J. M. Gregory, and W. M. Washington, 2005: Penetration of human-induced warming into the world's oceans. *Science*, **309**, 284–287, https://doi.org/10.1126/science.1112418.

Bellomo, K., V. L. Meccia, R. D'Agostino, F. Fabiano, S. M. Larson, J. von Hardenberg, and S. Corti, 2023: Impacts of a weakened AMOC on precipitation over the Euro-Atlantic region in the EC-Earth3 climate model. *Climate Dyn.*, 3397–3416, https://doi.org/10.1007/s00382-023-06754-2.

Biló, T. C., R. C. Perez, S. Dong, W. Johns, and T. Kanzow, 2024: Weakening of the Atlantic Meridional Overturning Circulation abyssal limb in the North Atlantic. *Nat. Geosci.*, **17**, 419–425, https://doi.org/10.1038/s41561-024-01422-4.

Buckley, M. W., and J. Marshall, 2016: Observations, inferences, and mechanisms of the Atlantic Meridional Overturning Circulation: A review. *Rev. Geophys.*, **54**, 5–63, https://doi.org/10.1002/2015RG000493.

Cheng, L., K. E. Trenberth, J. Fasullo, T. Boyer, J. Abraham, and J. Zhu, 2017: Improved estimates of ocean heat content from 1960 to 2015. *Sci. Adv.*, **3**, e1601545, https://doi.org/10.1126/sciadv.1601545.

——, and Coauthors, 2020: Record-setting ocean warmth continued in 2019. *Adv. Atmos. Sci.*, **37**, 137–142, https://doi.org/10.1007/s00376-020-9283-7.

——, and Coauthors, 2022: Past and future ocean warming. *Nat. Rev. Earth Environ.*, **3**, 776–794, https://doi.org/10.1038/s43017-022-00345-1.

Chidichimo, M. P., and Coauthors, 2023: Energetic overturning flows, dynamic interocean exchanges, and ocean warming observed in the South Atlantic. *Commun. Earth Environ.*, **4**, 10, https://doi.org/10.1038/s43247-022-00644-x.

Danabasoglu, G., and Coauthors, 2014: North Atlantic simulations in Coordinated Ocean-ice Reference Experiments phase II (CORE-II). Part I: Mean states. *Ocean Modell.*, **73**, 76–107, https://doi.org/10.1016/j.ocemod.2013.10.005.

——, and Coauthors, 2020: The Community Earth System Model version 2 (CESM2). *J. Adv. Model. Earth Syst.*, **12**, e2019MS001916, https://doi.org/10.1029/2019MS001916.

——, F. S. Castruccio, R. J. Small, R. Tomas, E. Frajka-Williams, and M. Lankhorst, 2021: Revisiting AMOC transport estimates from observations and models. *Geophys. Res. Lett.*, **48**, e2021GL093045, https://doi.org/10.1029/2021GL093045.

Deser, C., A. Phillips, V. Bourdette, and H. Teng, 2012: Uncertainty in climate change projections: The role of internal variability. *Climate Dyn.*, **38**, 527–546, https://doi.org/10.1007/s00382-010-0977-x.

——, and Coauthors, 2020: Insights from Earth system model initial-condition large ensembles and future prospects. *Nat. Climate Change*, **10**, 277–286, https://doi.org/10.1038/s41558-020-0731-2.

Dong, S., G. Goni, R. Domingues, F. Bringas, M. Goes, J. Christophersen, and M. Baringer, 2021: Synergy of in situ and satellite ocean observations in determining meridional heat transport in the Atlantic Ocean. *J. Geophys. Res. Oceans*, **126**, e2020JC017073, https://doi.org/10.1029/2020JC017073.

Frajka-Williams, E., and Coauthors, 2019: Atlantic Meridional Overturning Circulation: Observed transport and variability. *Front. Mar. Sci.*, **6**, 260, https://doi.org/10.3389/fmars.2019.00260.

Gregory, J. M., and Coauthors, 2005: A model intercomparison of changes in the Atlantic thermohaline circulation in response to increasing atmospheric CO_2 concentration. *Geophys. Res. Lett.*, **32**, L12703, https://doi.org/10.1029/2005GL023209.

Großelindemann, H., F. S. Castruccio, G. Danabasoglu, and A. Biastoch, 2025: Long-term variability and trends in the Agulhas Leakage and its impacts on the global overturning. *Ocean Sci.*, **21**, 93–112, https://doi.org/10.5194/os-21-93-2025.

Hu, S., S.-P. Xie, and W. Liu, 2020: Global pattern formation of net ocean surface heat flux response to greenhouse warming. *J. Climate*, **33**, 7503–7522, https://doi.org/10.1175/JCLI-D-19-0642.1.

Ivanciu, I., K. Matthes, A. Biastoch, S. Wahl, and J. Harlaß, 2021: Twenty-first-century Southern Hemisphere impacts of ozone recovery and climate change from the stratosphere to the ocean. *Wea. Climate Dyn.*, **3**, 139–171, https://doi.org/10.5194/wcd-3-139-2022.

Jackson, L. C., K. A. Peterson, C. D. Roberts, and R. A. Wood, 2016: Recent slowing of Atlantic overturning circulation as a recovery from earlier strengthening. *Nat. Geosci.*, **9**, 518–522, https://doi.org/10.1038/ngeo2715.

Kuhlbrodt, T., A. Griesel, M. Montoya, A. Levermann, M. Hofmann, and S. Rahmstorf, 2007: On the driving processes of the Atlantic meridional overturning circulation. *Rev. Geophys.*, **45**, RG2001, https://doi.org/10.1029/2004RG000166.

Larocca, L. J., and Coauthors, 2023: Greenland-wide accelerated retreat of peripheral glaciers in the twenty-first century. *Nat. Climate Change*, **13**, 1324–1328, https://doi.org/10.1038/s41558-023-01855-6.

Lee, S.-K., W. Park, E. Van Sebille, M. O. Baringer, C. Wang, D. B. Enfield, S. G. Yeager, and B. P. Kirtman, 2011: What caused the significant increase in Atlantic Ocean heat content since the mid-20th century? *Geophys. Res. Lett.*, **38**, L17607, https://doi.org/10.1029/2011GL048856.

Lee, T., and J. Marotzke, 1998: Seasonal cycles of meridional overturning and heat transport of the Indian Ocean. *J. Phys. Oceanogr.*, **28**, 923–943, https://doi.org/10.1175/1520-0485(1998)028<0923:SCOMOA>2.0.CO;2.

Li, Q., M. H. England, A. M. Hogg, S. R. Rintoul, and A. K. Morrison, 2023: Abyssal ocean overturning slowdown and warming driven by Antarctic meltwater. *Nature*, **615**, 841–847, https://doi.org/10.1038/s41586-023-05762-w.

Liu, W., A. V. Fedorov, S.-P. Xie, and S. Hu, 2020: Climate impacts of a weakened Atlantic Meridional Overturning Circulation in a warming climate. *Sci. Adv.*, **6**, eaaz4876, https://doi.org/10.1126/sciadv.aaz4876.

Ma, X., W. Liu, N. J. Burls, C. Chen, J. Cheng, G. Huang, and X. Li, 2021: Evolving AMOC multidecadal variability under different CO_2 forcings. *Climate Dyn.*, **57**, 593–610, https://doi.org/10.1007/s00382-021-05730-y.

Majumder, S., C. Schmid, and G. Halliwell, 2016: An observations and model-based analysis of meridional transports in the South Atlantic. *J. Geophys. Res. Oceans*, **121**, 5622–5638, https://doi.org/10.1002/2016jc011693.

Marcello, F., M. Tonelli, B. Ferrero, and I. Wainer, 2023: Projected Atlantic overturning slow-down is to be compensated by a strengthened South Atlantic subtropical gyre. *Commun. Earth Environ.*, **4**, 92, https://doi.org/10.1038/s43247-023-00750-4.

Marshall, J., A. Donohoe, D. Ferreira, and D. McGee, 2014: The ocean's role in setting the mean position of the Inter-Tropical Convergence Zone. *Climate Dyn.*, **42**, 1967–1979, https://doi.org/10.1007/s00382-013-1767-z.

Mecking, J. V., and S. S. Drijfhout, 2023: The decrease in ocean heat transport in response to global warming. *Nat. Climate Change*, **13**, 1229–1236, https://doi.org/10.1038/s41558-023-01829-8.

Mehling, O., K. Bellomo, M. Angeloni, C. Pasquero, and J. von Hardenberg, 2023: High-latitude precipitation as a driver of multicentennial variability of the AMOC in a climate model of intermediate complexity. *Climate Dyn.*, **61**, 1519–1534, https://doi.org/10.1007/s00382-022-06640-3.

Meinshausen, M., and Coauthors, 2020: The shared socioeconomic pathway (SSP) greenhouse gas concentrations and their extensions to 2500. *Geosci. Model Dev.*, **13**, 3571–3605, https://doi.org/10.5194/gmd-13-3571-2020.

Millan, R., E. Jager, J. Mouginot, M. H. Wood, S. H. Larsen, P. Mathiot, N. C. Jourdain, and A. Bjørk, 2023: Rapid disintegration and weakening of ice shelves in North Greenland. *Nat. Commun.*, **14**, 6914, https://doi.org/10.1038/s41467-023-42198-2.

Murphy, L. N., J. M. Klavans, A. C. Clement, and M. A. Cane, 2021: Investigating the roles of external forcing and ocean circulation on the Atlantic multidecadal SST variability in a large ensemble climate model hierarchy. *J. Climate*, **34**, 4835–4849, https://doi.org/10.1175/JCLI-D-20-0167.1.

O'Neill, B. C., and Coauthors, 2016: The Scenario Model Intercomparison Project (ScenarioMIP) for CMIP6. *Geosci. Model Dev.*, **9**, 3461–3482, https://doi.org/10.5194/gmd-9-3461-2016.

Pontes, G. M., and L. Menviel, 2024: Weakening of the Atlantic Meridional Overturning Circulation driven by subarctic freshening since the mid-twentieth century. *Nat. Geosci.*, **17**, 1291–1298, https://doi.org/10.1038/s41561-024-01568-1.

Povea-Pérez, Y., É. Guilyardi, A. V. Fedorov, and B. Ferster, 2024: The central role of the Atlantic Meridional Overturning Circulation in the Bjerknes compensation. *Climate Dyn.*, **62**, 575–587, https://doi.org/10.1007/s00382-023-06926-0.

Rodgers, K. B., and Coauthors, 2021: Ubiquity of human-induced changes in climate variability. *Earth Syst. Dyn.*, **12**, 1393–1411, https://doi.org/10.5194/esd-12-1393-2021.

Sancho, L. M. B., L. P. de Freitas Assad, and L. Landau, 2015: Volume and heat transports analysis in the South Atlantic Basin related to climate change scenarios. *Braz. J. Geophys.*, **33**, 333–348, https://doi.org/10.22564/rbgf.v33i2.724.

Schneider, T., T. Bischoff, and G. H. Haug, 2014: Migrations and dynamics of the intertropical convergence zone. *Nature*, **513**, 45–53, https://doi.org/10.1038/nature13636.

Sévellec, F., A. V. Fedorov, and W. Liu, 2017: Arctic sea-ice decline weakens the Atlantic Meridional Overturning Circulation. *Nat. Climate Change*, **7**, 604–610, https://doi.org/10.1038/nclimate3353.

Trenberth, K. E., and A. Solomon, 1994: The global heat balance: Heat transports in the atmosphere and ocean. *Climate Dyn.*, **10**, 107–134, https://doi.org/10.1007/BF00210625.

——, and J. M. Caron, 2001: Estimates of meridional atmosphere and ocean heat transports. *J. Climate*, **14**, 3433–3443, https://doi.org/10.1175/1520-0442(2001)014<3433:EOMAAO>2.0.CO;2.

——, Y. Zhang, J. T. Fasullo, and L. Cheng, 2019: Observation-based estimates of global and basin ocean meridional heat transport time series. *J. Climate*, **32**, 4567–4583, https://doi.org/10.1175/JCLI-D-18-0872.1.

Van Westen, R. M., M. Kliphuis, and H. A. Dijkstra, 2024: Physics-based early warning signal shows that AMOC is on tipping course. *Sci. Adv.*, **10**, eadk1189, https://doi.org/10.1126/sciadv.adk1189.

Wang, C., L. Zhang, S.-K. Lee, L. Wu, and C. R. Mechoso, 2014: A global perspective on CMIP5 climate model biases. *Nat. Climate Change*, **4**, 201–205, https://doi.org/10.1038/nclimate2118.

Xie, S.-P., C. Deser, G. A. Vecchi, J. Ma, H. Teng, and A. T. Wittenberg, 2010: Global warming pattern formation: Sea surface temperature and rainfall. *J. Climate*, **23**, 966–986, https://doi.org/10.1175/2009JCLI3329.1.